Dynamic Reconstruction of In-plane Strain Maps Using a Two-dimensional Sensing Skin

AUSTIN DOWNEY, JIN YAN, SIMON LAFLAMME and AN CHEN

ABSTRACT

Damage detection and localization in large-scale systems requires the detection of local faults over a typically very large geometry. This can be done through the deployment of two-dimensional sensor arrays capable of discreetly monitoring local changes over a structure's global area. The authors have previously developed a soft-elastomeric capacitor (SEC) thin film sensor capable of measuring the additive strain components over a surface along its two principal directions. For applications to structural health monitoring, it is useful to decompose the signal into strain components along these principal directions. When deployed in a dense sensor network configuration, the principal strain components can be extracted from the measured additive strain using a previously developed algorithm that used assumptions on the boundary conditions. The introduction of mature off-the-shelf solutions, for the purpose of boundary condition updating, has been shown to significantly improve the algorithm's accuracy. The newly created hybrid dense sensor network (HDSN), consisting of SECs and resistive strain gauges, is capable of producing orthogonal strain maps over the structure's surface. Previous studies were conducted using static loads. Here, the authors report on the capability of the HDSN-based technique to reconstruct dynamic strain maps for a component exposed to dynamic loads. Results demonstrate that the hybrid dense sensor network can efficiently reconstruct dynamic in-plane strain maps. These dynamic strain maps can then be used for the reconstruction of dynamic deflection shapes or, in combination with other damage detection algorithms, to detect, localize and quantify damage.

INTRODUCTION

Cost effective monitoring solutions for mesoscale structures, such as transportation infrastructures and energy systems, need to be capable of monitoring the structure's global (e.g., loss in stiffness) and local (e.g., crack propagation) conditions.

Austin Downey, Dept. of Civil, Constr. and Env. Eng,. Iowa State University, USA
Jin Yan, Dept. of Civil, Constr. and Env. Eng,. Iowa State University, USA
Simon Laflamme, Dept. of Civil, Constr. and Env. Eng,. Iowa State University, USA
An Chen, Dept. of Civil, Constr. and Env. Eng,. Iowa State University, USA

However, distinguishing between localized and global faults on a mesoscale system using state-of-the-art sensing technologies is difficult [1]. A solution to this global/local condition monitoring problem is the deployment of dense sensor networks (DSNs) that are capable of economically covering the structure's global surface. For example, a DSN of strain gauges can provide valuable information regarding deformation and stress distribution and can be used for the structural health monitoring of civil structures where damage is a localized phenomenon [2].

Various strain transducers have been adopted for monitoring of civil infrastructures, including resistive strain gauges (RSG), vibrating wire gauges, and fiber Bragg grating sensors. A limiting factor of these off-the-shelf sensors is their lack of scalability for measuring strain of a large surface. An advancement in strain sensing technologies has been proposed in the form of sensing skins [3, 4]. Deployed in an array over large areas, sensing skins offer many potential advantages over conventional point-based strain sensors. Examples of experimentally validated sensing skins include: a carbon nanotube (CNT) based strain sensors in the form of bucky paper [5]; a carbon nanotube-polymer composite patterned onto a flexible polyimide substrate with fully integrated data acquisition [6] and a strain sensing sheet constructed as a large area electronic from resistive strain gauges for crack detection and localization [7].

Within the scope of sensing skins, the authors have previously developed a capacitance-based sensor, termed soft elastomeric capacitor (SEC) [4] suitable for use in the monitoring of mesoscale systems. The SEC is a large area electronic that measures the additive in-plane strain of a substrate to which it is attached. Prior results have demonstrated the effectiveness of SECs for detecting fatigue cracks [8] and when deployed in a network for monitoring a structure's global condition [9]. To fully enable the applications of SECs for condition assessment of mesoscale structures, an algorithm to decompose the SEC's additive strain into uni-directional strain components, through leveraging a network of SECs, has been developed. Termed the extended least squares estimator (LSE) algorithm, it functions based on the introduction of resistive strain gauges (RSGs) into a network of SECs to enforce the boundary conditions within the DSN. The new sensor network consisting of SECs and RSGs is termed hybrid dense network (HDSN) [10]. This work seeks to expand on previous work by demonstrating that an HDSN consisting of SECs and RSGs is capable of efficiently reconstructing dynamic in-plane strain maps. This work expands the use of the previously proposed HDSN into dynamic excitations and demonstrates that the decomposed uni-directional in-plane strain maps can be used for reconstructing the deflection shapes.

BACKGROUND

Soft Elastomeric Capacitor

The SEC is a large area capacitor that transduces a change in geometry (i.e., strain) into a measurable change in capacitance. The sensor's capability to function as a large area electronic for structural health monitoring has been well documented and

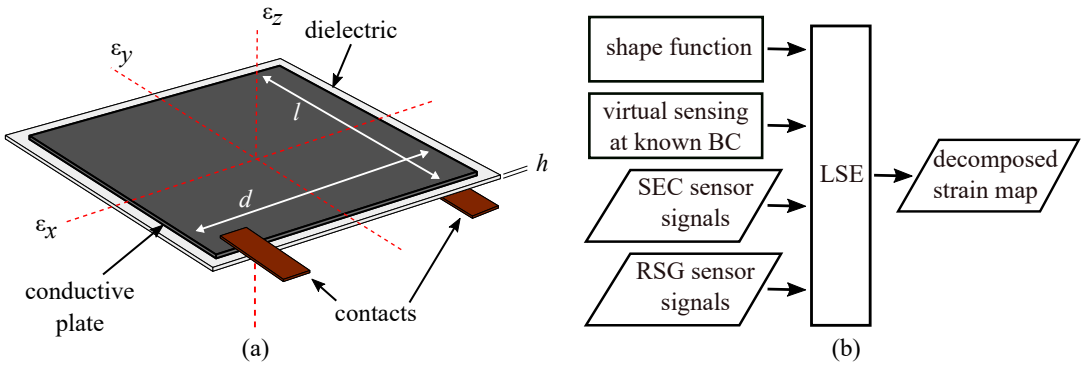

Figure 1. SEC sensors used in the deployment of an HDSN: (a) annotated SEC sensor with reference axes; and (b) diagrammed extended LSE algorithm for developing unidirectional strain maps.

is reviewed here for brevity. Its fabrication processes [4] and sensor characterization for static and dynamic [11] characterization have been previously reported.

The SEC measures the additive in-plane strain ($x - y$ plane in Figure 1(a)) of a monitored substrate. The sensor is pre-stretched during its installation to enable the measurement of tension and compression. Assuming a low sampling rate (< 1 kHz), the SEC is modeled as a non-lossy capacitor where capacitance (C) is given by the equation for a parallel plate capacitor $C = e_0 e_r \frac{A}{h}$ where $e_0 = 8.854$ pF/m is the vacuum permittivity, e_r is the polymer relative permittivity. The area of the plate, is given by $A = d \cdot l$, is the sensor area of width d and length l, and h is the thickness of the dielectric, as annotated in Figure 1(a). Assuming that the monitored substrate experiences only small, in-plane strains, an expression relating the sensor's change to is capacitance is expressed as

$$\frac{\Delta C}{C} = \lambda(\varepsilon_x + \varepsilon_y) \tag{1}$$

where λ represents the gauge factor with $\lambda \approx 2$ [11]. Equation (1) shows that the signal of the SEC varies as a function of the additive strain $\varepsilon_x + \varepsilon_y$.

Strain Decomposition Algorithm

An algorithm was designed to decompose the SEC signal (Equation (1)) into unidirectional strain components by leveraging an HDSN configuration of SECs and resistive strain gauges (RSG). The algorithm requires the knowledge of boundary conditions that can be either assumed, enforced through the measurement of strain at key locations, or a combination of both [10]. The algorithm uses measured point strain at key locations using off-the-shelf strain sensors, and is termed extended LSE algorithm. It is diagrammed in Figure 1(b) and briefly summarized in what follows.

The extended LSE algorithm works through assuming a polynomial displacement shape function w along the x-y plane such that $w(x, y) = \sum_{i=1,j=1}^{p} b_{ij} x^i y^j$, for a pth order polynomial. Here $b_{i,j}$ are regression coefficients that will be solved using an

LSE estimator. Considering an HDSN that includes both SECs and RSGs, the uni-directional strain at the location of each sensor node can be calculated through the enforcement of Kirchhoff's plate theory

$$\varepsilon_x(x,y) = -\frac{c}{2}\frac{\partial^2 w(x,y)}{\partial x^2} = \mathbf{\Gamma}_{\mathrm{x}}\mathbf{H}_{\mathrm{x}}\mathbf{B}_{\mathrm{x}} \tag{2}$$

$$\varepsilon_y(x,y) = -\frac{c}{2}\frac{\partial^2 w(x,y)}{\partial y^2} = \mathbf{\Gamma}_{\mathrm{y}}\mathbf{H}_{\mathrm{y}}\mathbf{B}_{\mathrm{y}} \tag{3}$$

where c is the thickness of the plate, $\mathbf{H}$ is the sensor placement matrix with $\mathbf{H} = [\mathbf{\Gamma}_{\mathrm{x}}\mathbf{H}_{\mathrm{x}}|\mathbf{\Gamma}_{\mathrm{y}}\mathbf{H}_{\mathrm{y}}]$ where $\mathbf{H}_{\mathrm{x}}$ and $\mathbf{H}_{\mathrm{y}}$ account for the SEC's additive strain measurements, $\mathbf{\Gamma}_x$ and $\mathbf{\Gamma}_y$ are diagonal weight matrices holding the scalar sensor weight values $\gamma_{x,k}$ and $\gamma_{y,k}$. For instance, corresponding rows in $\gamma_{x,k}$ and $\gamma_{y,k}$ would contain 1 and 1 for a bidirectional SEC, 1 and 0 for an RSG measuring ε_x, and 0 and 1 for an RSG measuring ε_y. An estimate for matrix $\mathbf{B}$, where $\mathbf{B} = [\mathbf{B}_{\mathrm{x}}|\mathbf{B}_{\mathrm{y}}]$, containing the regression coefficients $b_{i,j}$ can be estimated using an LSE:

$$\hat{\mathbf{B}} = (\mathbf{H}^T\mathbf{H})^{-1}\mathbf{H}^T\mathbf{S} \tag{4}$$

where the hat denotes an estimation. Thereafter, the estimated strain maps can be reconstructed with $\hat{\mathbf{E}}_{\mathrm{x}} = \mathbf{\Gamma}_{\mathrm{x}}\mathbf{H}_{\mathrm{x}}\hat{\mathbf{B}}_{\mathrm{x}}$ and $\hat{\mathbf{E}}_{\mathrm{y}} = \mathbf{\Gamma}_{\mathrm{y}}\mathbf{H}_{\mathrm{y}}\hat{\mathbf{B}}_{\mathrm{y}}$ where $\hat{\mathbf{E}}_{\mathrm{x}}$ and $\hat{\mathbf{E}}_{\mathrm{y}}$ are vectors containing the estimated strain at each sensor node in the x and y directions.

METHODOLOGY

An HDSN consisting of 40 SECs and 8 RSGs was deployed onto the surface of an aluminum plate of geometry 500 $\times$ 900 $\times$ 1.3 mm^3, as shown in Figure 2(a). In total, 40 RSGs were deployed onto the plate used for validation, with 8 of these used in the HDSN as shown in Figure 2(b). The left-hand side of the plate is attached to a rigid support (12.7 $\times$ 76.2 $\times$ 500 mm^3) with bolts that form a pinned connection. The right-hand side of the plate is restrained in the vertical direction through the use of two greased rods (12.7 mm) mounted between aluminum frames to form a roller connection. Each SEC covers 38 $\times$ 38 mm^2 and they are deployed in a 5 $\times$ 8 grid array. The point node used in constructing the $\mathbf{H}$ matrix is taken at the center of each SEC. RSGs used in the experimental setup are foil-type strain gauges with a gauge length of 6 mm and are manufactured by Tokyo Sokki Kenkyujo, model FLA-6-23-3LJBT. They are dual channel gauges, with each channel individually measuring ε_x and ε_y. SEC and RSG data are sampled simultaneously at 22 Samples per second using a custom-built data acquisition system.

In this work, a single 20-second test was used for the analysis of the HDSN's capability to reconstruct dynamic in-plane strain maps. A stepper motor, mounted under the HDSN test bench, was used to apply a 15 mm sinusoidal displacement at a rate of 0.25 Hz. No filtering or post processing was applied to the SEC or RSG data. A 6th order polynomial displacement function w was used in decomposing the uni-directional strain maps.

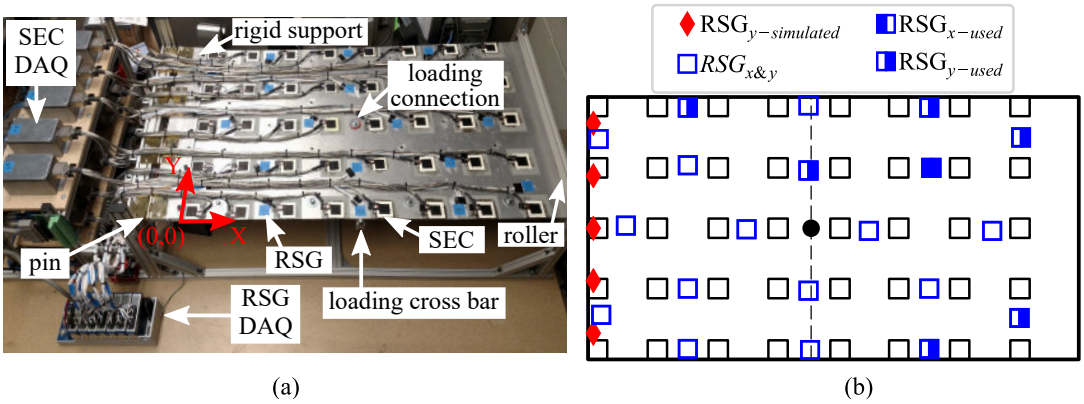

(a) (b)

Figure 2. Experimental setup used for dynamic strain map reconstruction with key components annotated: (a) picture of the test bench as tested with key components annotated; (b) schematic of the test bench showing the sensor locations with RSG sensors used in the HDSN denoted with the appropriately filled square.

The placement of RSGs within the HDSN for the purpose of enforcing boundary conditions has been shown to greatly affect the capability of the extended LSE algorithm to accuracy reproduce a structure's strain fields [10]. To reduce the error present in the reconstructed strain shape, a genetic algorithm with a learning gene pool was developed for selecting RSGs within a grid of SECs. This algorithm was previously developed by the authors and is implemented here [12]. Figure 2(b) denotes the 8 RSGs used in the HDSN, as selected by the genetic algorithm after a 250 generation investigation, using the data from the 20-second test. In all, 1 RSGs measuring ε_x and 7 RSG ε_y measuring were selected. Additionally, 5 pre-selected virtual RSGs were placed along the edge of the plate next to the reinforcement bar where boundary conditions can be assumed with a high level of certainty.

RESULTS AND DISCUSSIONS

The capability of the HDSN and extended LSE-based algorithm to reproduce the dynamic in-plane strain maps of the test bench is investigated with results shown in Figure 3. Figure 3(a)-(b) show the uni-directional strain field decomposed from the sensor data at the first positive peak of displacement, approximately 3 seconds into the test. These results show that the HDSN is capable of decomposing the SEC's additive strain into uni-directional strain maps over the plate's monitored area. The white area outside the HDSN was intentionally left blank as the interpolation of strain fields outside the HDSN was deemed inappropriate in this context. Figure 3(c) reports the mean absolute strain, as obtained through comparing the RSG data to the reconstructed strain map. As expected, ε_x experiences a greater absolute error than ε_y due to the higher strain levels in the x direction as denoted in Figure 2(a). The mean error values for ε_x and ε_y over the entire test is represented as a horizontal dashed line in Figure 3(c), the values are non-zero as error is taken as the absolute value. The error

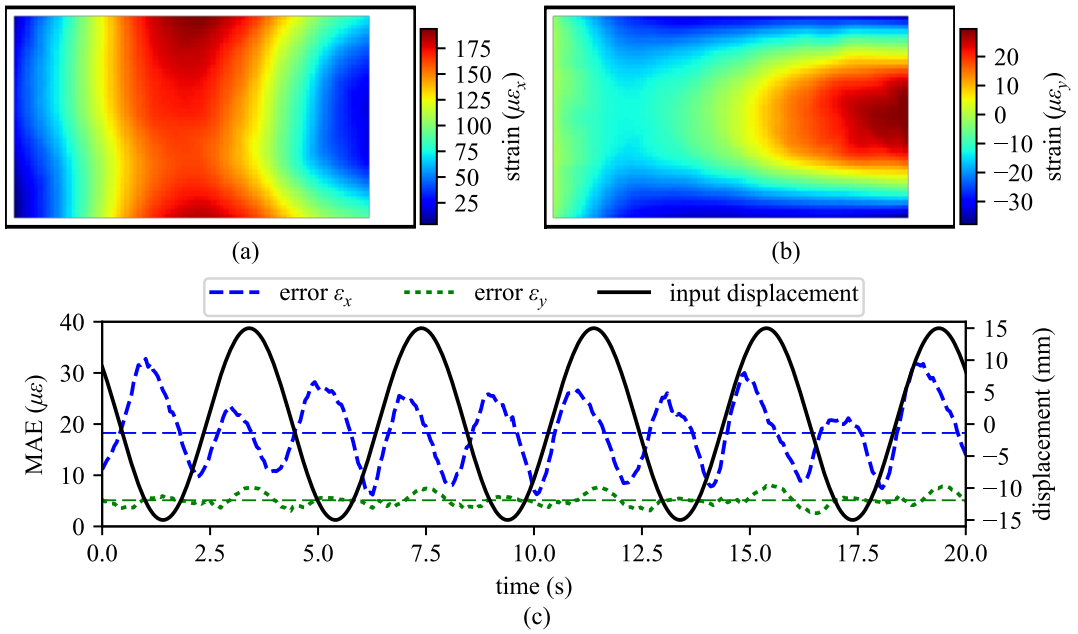

Figure 3. uni-directional in-plane strain maps reconstructed from the HDSN using the extended LSE algorithm showing: (a) ε_x ; (b)ε_y; and (c) error for ε_x and ε_y along with the input displacement.

in the x direction equates to 9.78 % error while the error in the y direction is 41.0 % error. The higher percent error in the y direction is a function of the overall lower strain values present in the decomposed y strain map. The level of error present in the system could be reduced by increasing the number of RSGs in the system. However, this would add complexity to the system and increase the cost associated with an HDSN.

Lastly, the strain maps reconstructed from the HDSN are used to calculate the vertical displacement at the loading connection (denoted in Figure 2(a)). The HDSN's calculated displacement is shown in Figure 4 in the form of a dashed blue line and is compared to the theoretical input displacement. The calculated displacement was achieved through applying two assumed boundary conditions and integrating the strain component of equation twice to obtain a displacement function. The assumed boundary conditions used for this validation were the slope of the plate at the loading connection taken equal to zero and the displacement of the plate at the right-hand side fixity taken equal to zero. Additionally, the absolute error between the input and calculated error is presented as a short-dashed red line. These results demonstrate that the HDSN can accurately reproduce the displacement of the plate.

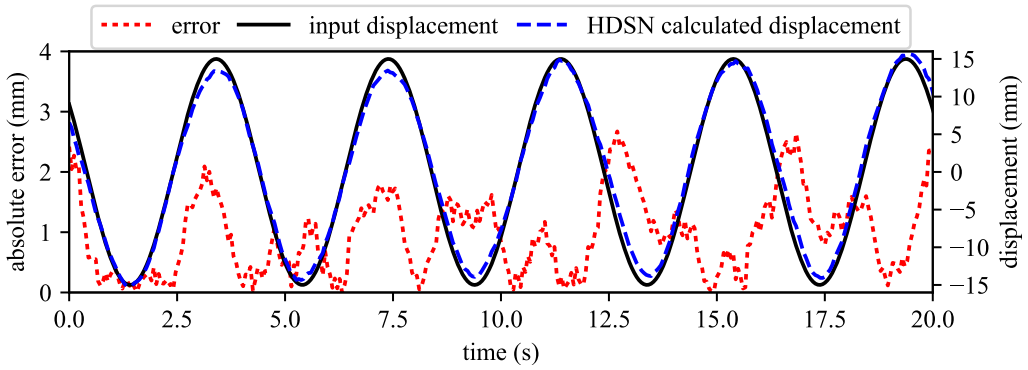

Figure 4. Displacement of the HDSN test bench showing the displacement for the input and HDSN calculated at the loading connection in the middle of the plate.

CONCLUSION

This paper presents the experimental validation of a novel hybrid dense sensor network (HDSN) for monitoring dynamic strain maps on a specially designed experimental test bench. The HDSN counted of 40 large area electronic sensors consisting of soft elastomeric capacitors (SECs), eight resistive strain gauges (RSGs), and assumed boundary condition along the rigid support. An algorithm based on a least squares estimator was used to fuse the SEC's additive strain measurements, the RSG's linear strain measurements, and the assumed boundary conditions into unidirectional strain maps for each time stamp of a 20-second test under a sinusoidal loading condition.

Experimental results demonstrated the capability of the HDSN to reconstruct the dynamic strain maps of the test plate with relatively low levels of error. Using the reconstructed strain maps and assumed boundary conditions, time-series deflection data was obtained and demonstrated that the HDSN can accuracy reproduce the plate's displacement. The HDSN technology shows promise for the structural health monitoring of very large structural components.

ACKNOWLEDGMENTS

This work is partly supported by the National Science Foundation Grant No. 1069283, which supports the activities of the Integrative Graduate Education and Research Traineeship (IGERT) in Wind Energy Science, Engineering and Policy (WESEP) at Iowa State University. Their support is gratefully acknowledged. Any opinions, findings, and conclusions or recommendations expressed in this material are those of the authors and do not necessarily reflect the views of the National Science Foundation.

References

1. S. D. Fassois and J. S. Sakellariou. Time-series methods for fault detection and identification in vibrating structures. *Philosophical Transactions of the Royal Society A: Mathematical, Physical and Engineering Sciences*, 365(1851):411–448, feb 2007.
2. Scott W. Doebling, Charles R. Farrar, and Michael B. Prime. A summary review of vibration-based damage identification methods. *The Shock and Vibration Digest*, 30:91–105, 1998.
3. Kenneth J. Loh and Faezeh Azhari. Recent advances in skin-inspired sensors enabled by nanotechnology. *JOM*, 64(7):793–801, jul 2012.
4. Simon Laflamme, Matthias Kollosche, Jerome J. Connor, and Guggi Kofod. Robust flexible capacitive surface sensor for structural health monitoring applications. *Journal of Engineering Mechanics*, 139(7):879–885, jul 2013.
5. Prasad Dharap, Zhiling Li, Satish Nagarajaiah, and Enrique V. Barrera. Flexural strain sensing using carbon nanotube film. *Sensor Review*, 24(3):271–273, sep 2004.
6. Andrew R. Burton, Masahiro Kurata, Hiromichi Nishino, and Jerome P. Lynch. Fully integrated patterned carbon nanotube strain sensors on flexible sensing skin substrates for structural health monitoring. In Jerome P. Lynch, editor, *Sensors and Smart Structures Technologies for Civil, Mechanical, and Aerospace Systems 2016*. SPIE, apr 2016.
7. Yao Yao and Branko Glisic. Detection of steel fatigue cracks with strain sensing sheets based on large area electronics. *Sensors*, 15(4):8088–8108, apr 2015.
8. Xiangxiong Kong, Jian Li, Caroline Bennett, William Collins, and Simon Laflamme. Numerical simulation and experimental validation of a large-area capacitive strain sensor for fatigue crack monitoring. *Measurement Science and Technology*, 27(12):124009, oct 2016.
9. Simon Laflamme, Liang Cao, Eleni Chatzi, and Filippo Ubertini. Damage detection and localization from dense network of strain sensors. *Shock and Vibration*, 2016:1–13, 2016.
10. Austin Downey, Simon Laflamme, and Filippo Ubertini. Reconstruction of in-plane strain maps using hybrid dense sensor network composed of sensing skin. *Measurement Science and Technology*, 27(12):124016, nov 2016.
11. Simon Laflamme, Filippo Ubertini, Hussam Saleem, Antonella D'Alessandro, Austin Downey, Halil Ceylan, and Annibale Luigi Materazzi. Dynamic characterization of a soft elastomeric capacitor for structural health monitoring. *Journal of Structural Engineering*, 141(8):04014186, aug 2015.
12. Austin Downey, Chao Hu, and Simon Laflamme. Optimal sensor placement within a hybrid dense sensor network using an adaptive genetic algorithm with learning gene pool. *Structural Health Monitoring*, page 147592171770253, apr 2017.